

Microresonators as promising building blocks for VLSI photonics

Alfred Driessen, Ronald Dekker, Mart B.J. Diemeer, Douwe H. Geuzebroek, Hugo J.W.M. Hoekstra, Edwin J. Klein and Arne Leinse
 Integrated Optical Microsystems, MESA⁺ Institute, University of Twente,
 P.O. Box 217, 7500 AE Enschede, The Netherlands

ABSTRACT

In the last years much effort has been taken to arrive at optical integrated circuits with high complexity and advanced functionality. For this aim high index contrast structures are employed that allow for a large number of functional elements within a given chip area: VLSI photonics. It is shown that optical microresonators can be considered as promising basic building blocks for filtering, amplification, modulation, switching and sensing. Active functions can be obtained by monolithic integration or a hybrid approach using materials with thermo-, electro- and opto-optic properties and materials with optical gain. Examples are mainly taken from work at MESA⁺.

Keywords: Integrated optics, optical microresonator, optical filter, optical add-drop node, optical modulator, optical sensor

1. INTRODUCTION

After several years of declining activities in the field of optical communications new optimistic voices can be heard triggered by the massive introduction of broadband access. Europe, the Middle East and Africa spent \$ 3.2 bn in optical networking over the year 2004, an increase of 53% with respect to 2003¹. This increase demonstrates that the up to now installed optical communication hardware is not sufficient and new investments are done.

Looking ahead in time, let's say 5 to 10 years, optical techniques will not only be used in the core-network but also in the METRO- and Access networks. The optical systems and devices needed for this will operate at several Gbit/s and will be compact to allow complex optical routing and data processing. Reliability will be an important issue as no trained personnel is available in a home or small enterprise environment. These optical systems will be low-cost, as the end user can not share costs, and can be classified as consumer photonics. The only answer to these challenges will be mass-produced very large scale integrated (VLSI) photonics in close analogy with the electronic VLSI electronic circuits.

waveguiding principle	index contrast	bend-radius	optical feedback	fiber-chip coupling	density [functions/cm ²]
index guiding	low, $\Delta n \sim 0.01$	5 mm	too slow	easy	1
index guiding	high, $\Delta n \sim 0.07$	500 μm	resonator	easy with small core fiber	25
index guiding	very high, $\Delta n \sim 0.5$	10 μm	micro-resonator	difficult, taper structures needed	1 000
index guiding	ultra-high, $\Delta n \sim 2$	1 μm	micro-resonator	very difficult	100 000
Bragg reflection (PBS)	ultra-high, $\Delta n \sim 2$	1 μm	micro-resonator	very difficult	100 000

Table 1: Characteristics of waveguide structures with increasing index contrast.

For high integration, the single functional elements in photonic devices should be small. In electronic ICs a state-of-the-art transistor has a diameter of 50 nm, in optical devices a lower limit is given by the relatively large wavelength of light in the order of 1000 nm. Another size limitation is given by the inherent losses of small-radius bends. Only by working with high index contrast waveguides, these losses can be reduced to an acceptable minimum. Table 1 gives the characteristics of waveguide structures with increasing index contrast. Packaging and fiber-chip coupling (giving rise to

70 to 80% of the total costs of an integrated optical device) is increasingly difficult with high contrast structures. With increasing density of optical functions on a chip, the cost per functional element, however, is rapidly decreasing.

The waveguiding principle considered here is total internal reflection on a single interface called index guiding. In the last decade another approach based on photonic band gap structures (PBS) is intensively studied. Index guiding structures are more close to market as an evolutionary path can be followed in contrast to PBSs that are only possible at ultra-high index contrast. It should also be mentioned that the structures in the three lowest rows in Table 1, with critical dimensions in the nanometer range, fall within the realm of nanophotonics.

The desired photonic components have to be compact, allowing active functions like switching and amplification and will make use of nanotechnology. Similar to the transistor in the electronic world one would like to have also a basic building block in photonics. Structures with optical feedback, for example resonators, could fulfill this role. In the following we will concentrate on microresonators^{2,3,4} based on high index contrast waveguiding structures and will show that they are promising building blocks for VLSI photonics. In section 2 we give an overview of the basic principles of microresonators. Thereafter an overview of the results is presented obtained in the EC-funded European IST NAIS project. In the 4th section a few examples are given of microresonators in new application fields: light sources and optical sensing. Finally a summary with short conclusions are given. The examples presented are mainly taken from own work often carried out in cooperation with others.

2. BASIC PRINCIPLES OF MICRORESONATORS

An optical microresonator is an integrated optics structure with optical feedback that allows a variety of functions like wavelength filter, optical switch or optical transistor⁵. Fig.1.a) gives a top view of such a device with two adjacent single mode port waveguides. Light enters at I_{in} and couples in part to the resonator. The rest of the power goes to $I_{through}$. Within the ring resonator the light propagates in a whispering gallery mode and couples partly to the output waveguide I_{drop} . After further propagation within the ring the light couples partly to $I_{through}$. Depending on the phase of the light after a roundtrip constructive or destructive interference will occur within the ring or $I_{through}$. In the case of constructive interference the resonator is on-resonance and the light coupled to $I_{through}$ has a phase shift of 180° with respect to I_{in} . Fig.1.b) gives schematically the resulting normalized spectral response of a loss-less, symmetric resonator to a constant power input signal with changing wavelength or alternatively changing phase in the resonator or changing effective index. The power $I_{through}$ is always equal to I_{in} with exception near to the resonance, in that case $I_{drop} = I_{in}$.

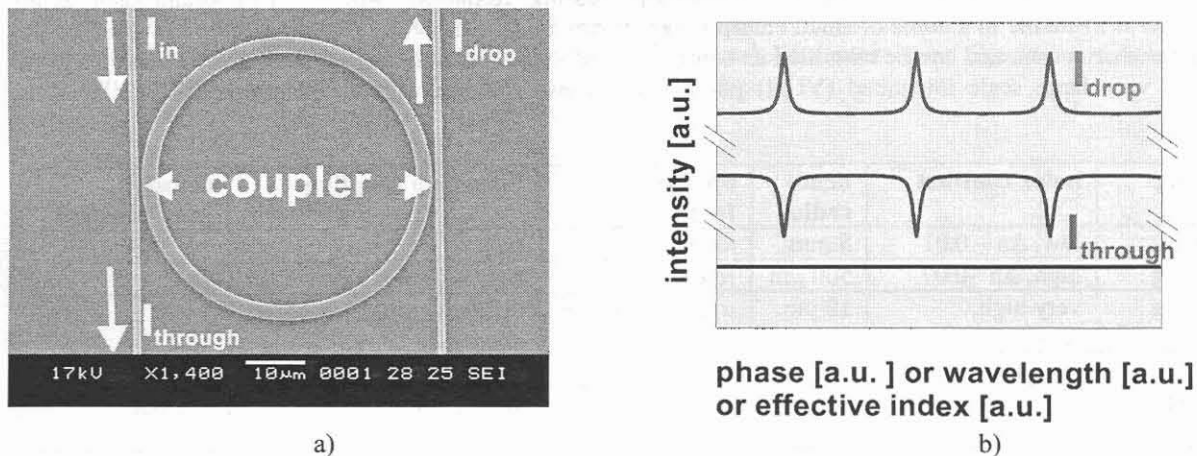


FIGURE 1: Microresonator with two adjacent waveguides serving as in- and output port; a) topview; b) schematic spectral response to a constant input intensity.

The performance of the microresonator is characterized by its Lorentzian lineshape of the resonance lines in the drop port that allows for a small 3dB bandwidth $\Delta\lambda_{3dB}$ but admits a poor rejection in the off-resonance condition. This becomes especially clear in a dB plot, see Fig.2. Also shown are the free spectral range (FSR) and the cross-talk level of -24 dB. A relative measure for the selectivity of the resonator is the finesse $F = FSR / \Delta\lambda_{3dB}$. The quality factor Q is given by $Q = \lambda / \Delta\lambda_{3dB}$, the cavity ring-down time $\tau_{cav} = \lambda Q / 2\pi c$ and the average number of roundtrips m of photons in a resonator $m = F / 2\pi$.

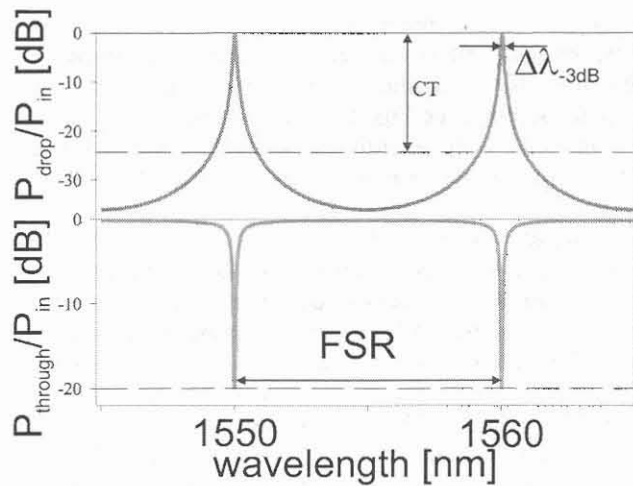


Figure 2: Example of the power in the drop and through port of a loss-less microresonator with $F \sim 100$ as a function of wavelength.

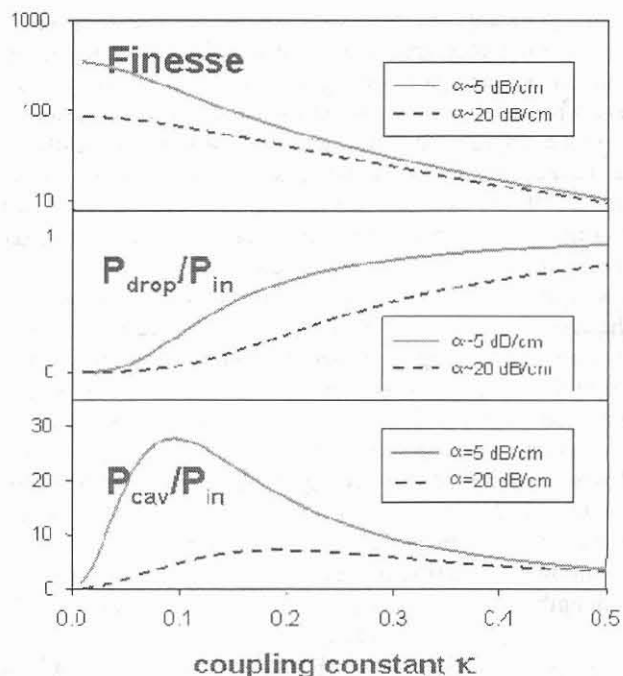


Figure 3: Finesse (logarithmic scale), normalized drop power and normalized cavity power as a function of the field coupling constant κ for a microresonator of radius $25 \mu\text{m}$.

For the design of a microresonator the field coupling constant κ between the port waveguides and the ringresonator plays an essential role. In a loss-less resonator with an infinite unloaded finesse the port waveguides introduce the load determined only by the coupling constant(s) κ . If the resonator has a certain propagation loss α , the resulting finesse, the normalized power in the drop channel $P_{\text{drop}}/P_{\text{in}}$ and the normalized power in the cavity waveguide $P_{\text{cav}}/P_{\text{in}}$ are largely varying functions of κ , see Fig. 3. For wavelength selectivity the finesse is the most relevant parameter and accordingly small coupling constants should be chosen. With regard to the drop efficiency even small losses will reduce P_{drop} completely for a weakly coupled resonator. Therefore highly coupled structures should be employed, which have, however, a reduced F and wavelength selectivity. For applications where high cavity fields are desired, e.g. all-optical data processing, P_{cav} shows a maximum at low losses and small κ .

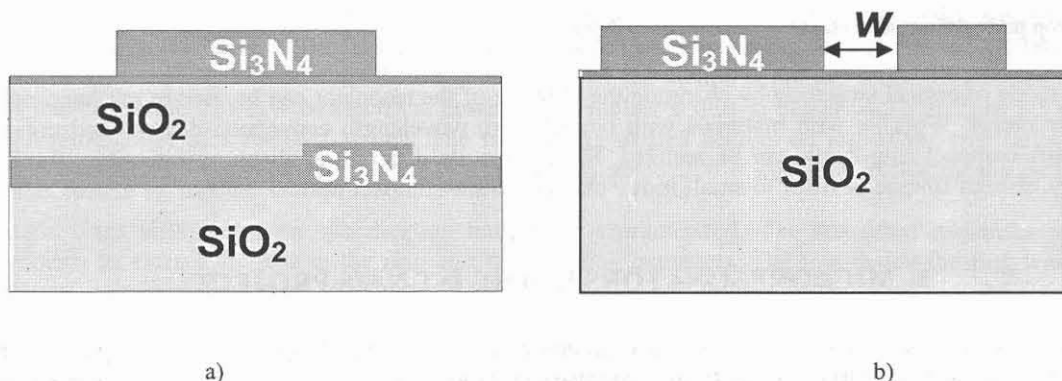


Figure 4: The two basic geometries for microresonators with port waveguides: a) vertical arrangement; b) lateral arrangement. The structure in this case is fabricated in silicon-based technology, with the index of refraction of SiO_2 and Si_3N_4 1.45 and 2.0 respectively

There are principally two solutions for the positioning of the adjacent waveguides with respect to the resonator: horizontal or vertical arrangement². In the vertical arrangement, Fig. 4.a), a two-step lithographic process is needed. The

coupling constants are mainly determined by the thickness and refractive index of the intermediate layer and the relative offsets of the underlying waveguides with respect to the ring. This approach allows also for an optimized independent choice for ring and port waveguides. Critical in the vertical arrangement is the alignment of the two lithographic steps, where a precision within 100 nm is needed. In the case of horizontal coupling, see Fig. 4.b), only a single lithographic step with a single mask is needed. The coupling is mainly determined by the width w of the gap between the straight and bent waveguides and demands nanometer precision in the case of high refractive index contrasts. There is reduced design flexibility as core layer and core thickness should be identical.

In Fig. 1.b. the spectral response of a microresonator as a function of wavelength has already been given. Just by changing the wavelength, the effective index or the phase, light can be directed either to the drop or the through port. In this way the device performs as a filter or space switch. There is another mode. If one considers a single resonance line in the drop port, the amplitude and width is determined by the roundtrip losses, see Fig. 5. By changing the losses and consequently reducing the Q-factor, light can effectively be switched between the two drop ports.

From the foregoing it is clear that the microresonator can carry out a large number of optical functions. It can be used as a compact filter with high resolution. For Wavelength Division Multiplexing (WDM) applications the unused input of the second port waveguide with the drop port can be considered as the add port. In this way an ultra-compact add-drop node can be realized. Switching of light -the optical analogue of a relais - can be done by changing the phase in the resonator by thermal, mechanical or electro-optical means. Electro-optic switching is especially attractive as with materials like polymers, modulation of signals exceeding 0.1 THz can be achieved⁶. Working with all-optical materials allowing the interaction of light by light, an optical transistor can be realized allowing bi-stability, light amplification, wavelength conversion and logic AND or OR functions⁷.

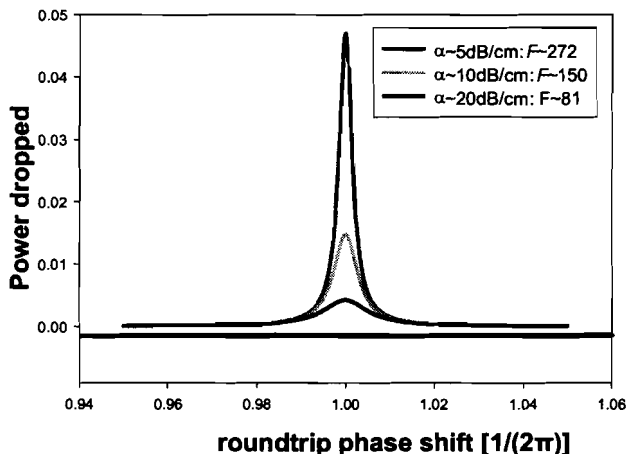


Figure 5: The drop power of a microresonator as a function of phase shift for different values of roundtrip losses, c.q. finesse.

The second mode of optical switching by changing the Q factor of the resonator can be used in mechano-optical⁸ and opto-optical structures. Working with materials with optical gain, wavelength conversion devices and coherent light sources and ultra-compact ring-lasers can be realized. Finally a quite different application is feasible. Exploiting the high sensitivity of high finesse cavities to small index changes, ultra-compact optical sensors⁹ or sensor arrays can be realized.

3. MICRORESONATORS IN THE IST NAIS PROJECT

In the recently finished EC-IST funded NAIS (Next Generation Active Integrated Optic Subsystem) project¹⁰ a number of European academic and industrial groups from 7 countries collaborated to apply active and passive microresonators in an optical transceiver for the access network. In the following three results are presented: (i) a compact wavelength-selective switch; (ii) a high-speed microrsonator-based electro-optic modulator, (iii) an ultra-compact reconfigurable add-drop multiplexer.

3.1 Wavelength-selective switch¹¹

The wavelength-selective switch is based on two MRs, as shown schematically in Fig. 6.a). The measured response of the two-stage switch in ON and OFF state is shown in Fig. 6.b). The first stage selects a certain wavelength band. By tuning the center wavelength of the second stage to overlap the center wavelength of the first stage, the wavelength band is switched to the drop port (ON-state). In the OFF-state, the center wavelength of the second stage does not overlap and the light dropped by the first ring is not used. The MRs are thermally tunable by means of a heater on top of the cladding. Driving the MRs thermally is fast enough for switching applications where submicrosecond responses are sufficient. Switching is possible up to several kilohertz¹² by optimization of the driving signal.

For applications in an access network, the switch is especially useful as it allows to select just one specific wavelength band and to disregard the others. The selectivity of the switch can be improved by using two different radii of the rings in the switch. In that case, the Vernier effect accounts for an increase in the total FSR up to 36 nm¹³. The switch can be a building block for even more complex structures like an array of switches which can switch different wavelength bands simultaneously.

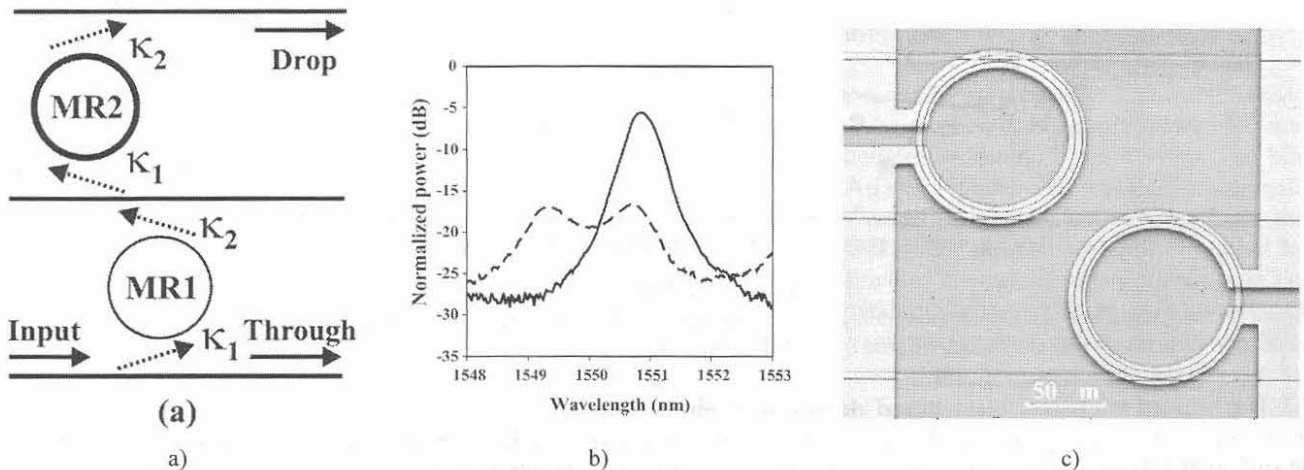


Figure 6: Wavelength selective switch based on 2 MRs; a) schematic view; b) measured response of switch: solid line: ON-state; dashed line: OFF-state; c) microscope photograph of a realized switch

An MR-based switch has been realized in SiO₂-Si₃N₄ technology¹⁴. The switch was made out of two MRs which are vertically coupled to the port waveguides. The port and ring waveguide dimensions are $2 \times 0.14 \mu\text{m}^2$ and $2.5 \times 0.18 \mu\text{m}^2$, respectively. The vertical separation between port and waveguide is 1 μm . Omega-shaped chromium heaters were applied on top of the device. The measured spectral responses of the switch in both the ON and OFF states are shown in Fig. 6.b). The responses are normalized to the measured power in the through port of the device while OFF-resonance and give, consequently, the on-chip IL in the drop port. The switch has a measured ON-OFF ratio of 12 dB and a channel separation better than 20 dB. The on-chip IL in the drop port of the switch is around 6 dB. The device was switched between ON and OFF using 225 mW of electrical power. This implies a shift in center wavelength of 6.5 pm/mW. Fig. 6.c) shows a photograph of a realized switch. The two omega-shaped heaters on top of the two rings and the port waveguides are clearly visible. The size of the switch itself is about $200 \times 200 \mu\text{m}^2$ excluding the pads to wire the heaters.

Also, single rings with the same specification have been characterized. The measured responses were fitted to analytical models to extract the loss in the ring and the coupling constants. The loss inside the ring was found to be about 5 dB/cm, corresponding to 0.16 dB/round-trip. The measured field coupling constants of 0.6 are in good agreement with the designed values. The propagation losses inside the straight waveguides are lower than 1 dB/cm. The on-chip IL in the drop port of a single ring is about 3 dB which is in accordance with the 6-dB IL in the switch.

Gigabit/s measurements on single rings with similar dimensions were performed with a LiNbO Mach-Zehnder modulator driven by a 10-Gb/s pseudorandom binary sequence generator to see the influence of the filter on the modulated nonreturn-to-zero (NRZ) signal. The group delay of the ring was measured by using the phase-shift method¹⁵. At resonance, the measured relative group delay is 7 ps, as is shown in Fig. 7. The measured 10-Gb/s modulation signal with a bit length of 100 ps is shown in the inlay of Fig. 5 where the eye responses are shown. The top eye diagram is obtained directly after the modulator, the bottom one after being filtered by the ring. The ring does not

degrade the modulated signal significantly as could be expected since the bandwidth was designed to be 50 GHz and the maximum group delay difference is much smaller than the duration of a single bit. The measured Q factor of the eye diagram of the filtered signal is about 7.5, leading to a theoretical bit-error rate of $< 10^{-12}$. The power penalty due to the single ring is 3 dB, since only the IL is of influence given this bit rate. As the complete wavelength selective switch is made out of two microrings, its group delay is twice the amount of the single ring, i.e. 14 ps at resonance.

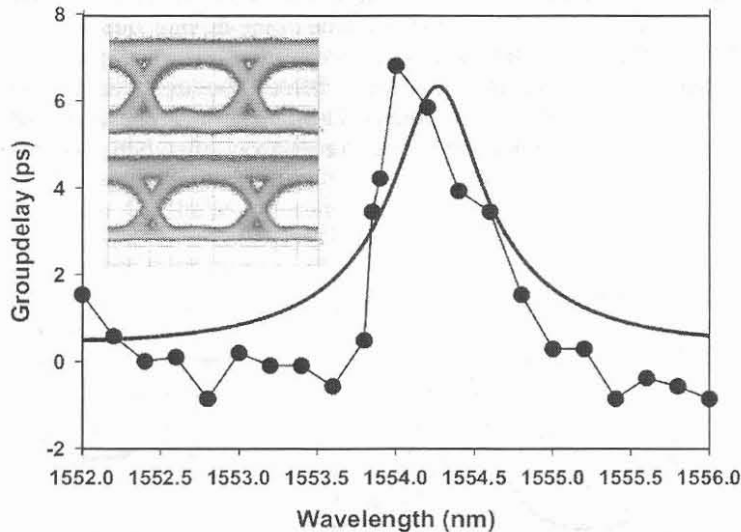


Figure 7: Measured and simulated groupdelay of a single MR. Also shown are the EYE diagrams of 10 Gbit/s NRZ signals of modulator output (top) and after being filtered by the MR (bottom).

3.2 High-speed microresonator-based electro-optic modulator¹⁶

In section 1.1 has already been explained that by changing the optical path within the ring its resonance wavelengths can be shifted and, both in the through- and drop port, an amplitude as well as phase modulation can be generated. For high-speed applications this change can be induced by an electric field obtained by sandwiching the MR between two electrodes. Because of their high electro-optic coefficients, polymers are very suitable for this type of devices¹⁷. One of the problems in realizing such a device in a vertical coupling arrangement is the position of the MR relative to the two port waveguides. This position determines the amount of light that couples from the waveguides to the ring (and vice versa) at both the through- and drop port side (the coupling constants). These coupling constants are critical parameters determining the spectral behavior. Coupling the MR to a single waveguide simplifies the fabrication process because there is only one coupling constant involved. In addition, the spectral behavior of the MR is less sensitive to changes in this single coupling constant. In an ideal lossless ring the through port spectrum has no resonance dips because no light is coupled to the drop port waveguide. In order to use a MR coupled to a single waveguide, the phase change around a resonance wavelength can be used. Fig. 8 shows schematically the output spectrum and the phase response of a slightly lossy MR around a resonance wavelength (λ_r).

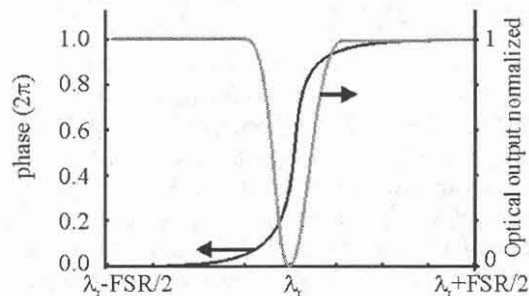


Figure 8: Output power and phase response of the through port waveguide around a resonance wavelength

This phase response can conveniently be converted to an intensity modulation by combination with a Mach Zehnder Interferometer (MZI). When switching between the on-resonance and off-resonance condition, the difference between the two branches of the MZI can switch from π to 0. This combination between a MR and MZI is shown (including a cross section through MR and waveguides) in Fig. 9.

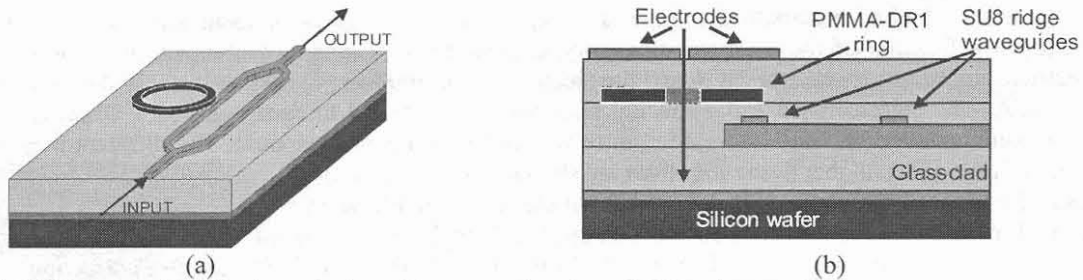


Figure 9: A MZI-ring device: (a) schematic view; (b) cross section through MR and waveguides

The complete device is fabricated in a polymer layerstack, which can be deposited by spin-coating. The material used for the 2 μm wide ridge waveguides is the negative photoresist SU8. The ridges have a height of approximately 300 nm. The ridge waveguides can be defined in a two-step lithographic process without any additional etching-step. The MR (with a radius of 150 μm) is fabricated in the nonlinear polymer PMMA-DR1 (synthesized by Ecole Nationale Supérieure de Chimie de Montpellier). The MR is defined by lithography followed by reactive ion etching. Both, the MR and the ridge waveguides, are surrounded by a methyl-silicone resin (sold under the name PS233 Glassclad by United Chemical Technologies). The splitter and combiner in the MZI are fabricated by making two y-junctions in the single mode waveguide. The part of the SU8 layer under the MR is removed lithographically in order to prevent coupling of light from the MR to this layer. Coupling to this layer would induce additional optical loss in the MR. Fabricating a balanced MZI is relatively easy when applying a heater over one of the branches. This branch can be tuned, such that both branches have the desired optical path length difference.

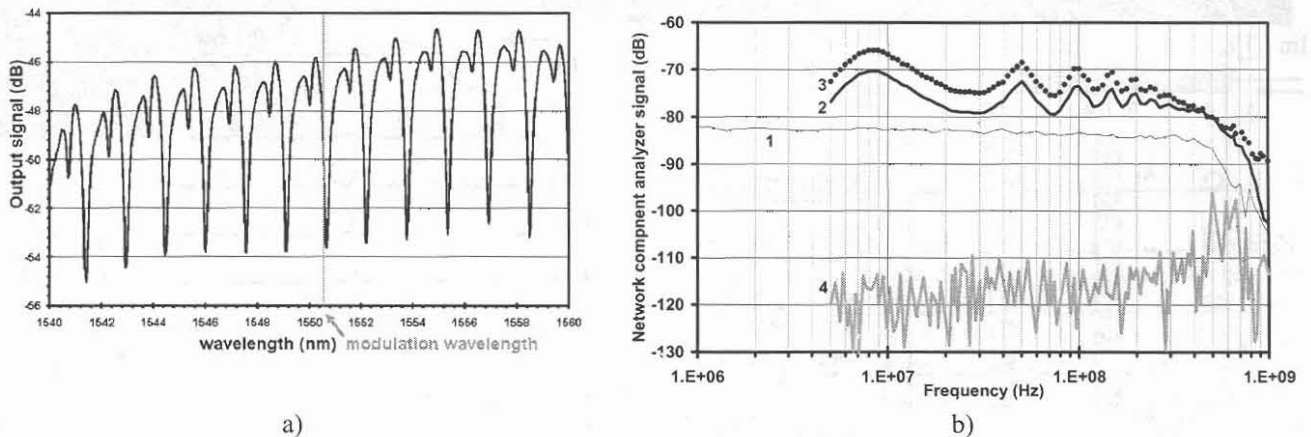


Figure 10: Experimental results of MR-MZI; a) spectral response (TE); the vertical line is the wavelength of the CW tunable laser at which modulation was measured; b) frequency spectrum.

While coupling in light at the input waveguide, the spectrum can be measured at the output waveguide. For the TE mode this spectrum shows two sets of resonance lines originating by two resonator modes, see figure 10.a). When using the MR as a modulator, this does not matter because a single input wavelength (on a flank of one of the steep dips) is chosen as a modulation wavelength. While applying a modulating voltage between top and bottom electrode, the amount of optical modulation is measured. Because the slope of the spectrum around the modulation wavelength is known, the induced wavelength shift of the spectrum can be calculated for a certain modulation ripple. From this wavelength shift, the change in the refractive index of the MR-material can be calculated and with the electric field applied known, the electro optic coefficient is determined. The r_{33} value found for this device is approximately 10 pm/V, which is in accordance to the values found in literature¹⁸. The electrode structure used is a lumped element structure

because the length of the electrodes above such a MR can be small. A rule of thumb in RF design states that an electrode can be used as a lumped element as long as its length is smaller than 10% of the wavelength of the electrical driving field. Even for electrode structures of 1 cm in length this corresponds to an electrical frequency as high as 2 GHz. The electrode size can even be reduced to the size of the MR, making frequencies of 60 GHz possible without special RF electrode design.

The frequency of the applied modulation voltage is changed by a network component analyzer (NCA) and the modulation depth as a function of the electrical frequency is determined. These measurements were done with and without an electrical amplifier between the NCA and the electrode. This amplifier is used to increase the limited voltage applied by the NCA. The detector used had a spectral response which started to decay around 1 GHz. This spectral response was measured and the measured device response was corrected for this response. The different measurements done are shown in figure 10.b). In this figure four lines are shown. These lines are:

1. Measured frequency response of the device without electrical amplification and detector correction
2. Measured frequency response of the device with electrical amplification and without detector correction
3. Measured frequency response of the device with electrical amplification and with detector correction
4. The noise signal of the detector (with the laser power off)

In lines 2 and 3 a modulation can be seen with a periodicity of 50 MHz. This is probably caused by the amplifier which gets reflections from the electrodes back. This modulation is not caused by the device because in line 1 the frequency response is flat. It can be seen that modulation frequencies up to 1 GHz can be measured. With this performance, data-rates exceeding 1 Gbit/s can be transmitted. With some specific modulation techniques data-rates of 2 to 3 Gbit/s will be possible.

3.3 An ultra-compact reconfigurable optical add-drop multiplexer¹⁹

An important component in which the filter function and small size of MRs can be applied effectively is a WDM router. Figure 1 shows a possible 4-channel implementation of such a router²⁰. This router consists of five 4-way Optical Add-Drop multiplexers (OADM). In this router the WDM input signal I_{in} is first separated into individual channels ($\lambda_1 \dots \lambda_4$) by an OADM. Each of these channels is then guided into one of four additional OADMs. These OADMs can then add these channels to one of four output waveguides I_{outx} .

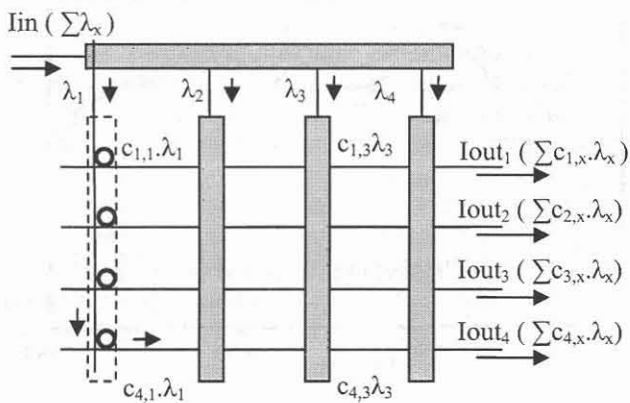


Figure 11: Schematic of a 4-channel WDM Router consisting of 5 connected OADM's

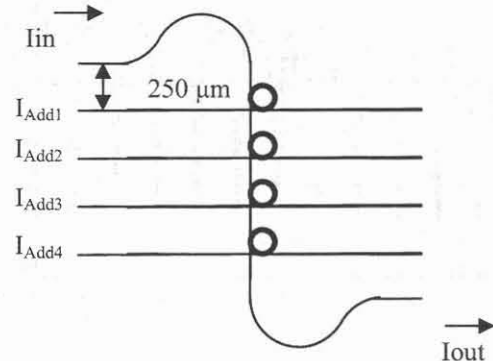


Figure 12: Lay-out of the realized ROADM

An OADM based on MRs offers several advantages over conventional implementations based on arrayed waveguide gratings or MZIs. The use of MRs allows for extremely small OADM implementations. In addition, a minimal component implementation of a 4-channel OADM based on MRs can already be realized with only four MRs, due to their highly selective filter characteristic. The first column of Figure 11 shows such an implementation where each MR drops an incoming channel λ_x to one of the outputs I_{outx} when its resonance frequency corresponds to that of the incoming channel. The OADM was designed as shown in Figure 12. It consists of a central waveguide (I_{in}/I_{out}) and four Add/Drop waveguides. These waveguides are spaced at 250 μm to allow for a standard fiber-array connection. The

size of the OADM, $1.25 \times 0.2 \text{ mm}^2$ is mainly determined by this spacing. A single MR is located at each intersection of central- and add-drop waveguides. The cross-grid waveguide approach²¹, in which the two waveguides that couple to the MR cross each other, leads to some crosstalk but is also the most efficient geometry for the OADM. Each of the four MRs can be thermally tuned by a heater. The heater is omega-shaped for high power efficiency. The MR has a radius of $50 \mu\text{m}$, a height of 190 nm and a width of $2.5 \mu\text{m}$, giving an $N_{\text{eff}}=1.517$ (TE @ 1550 nm). The $50 \mu\text{m}$ radius was chosen because it gives a FSR that is smaller than the thermal tuning range, allowing full FSR tuning. In addition, it allows for a MR that is nearly phase matched to the port waveguides. The MR is vertically coupled to these port waveguides which are $2 \mu\text{m}$ wide, 140 nm high and have a $N_{\text{eff}}=1.505$ (TE@ 1550 nm). Both the MR and the port waveguides are designed for TE operation.

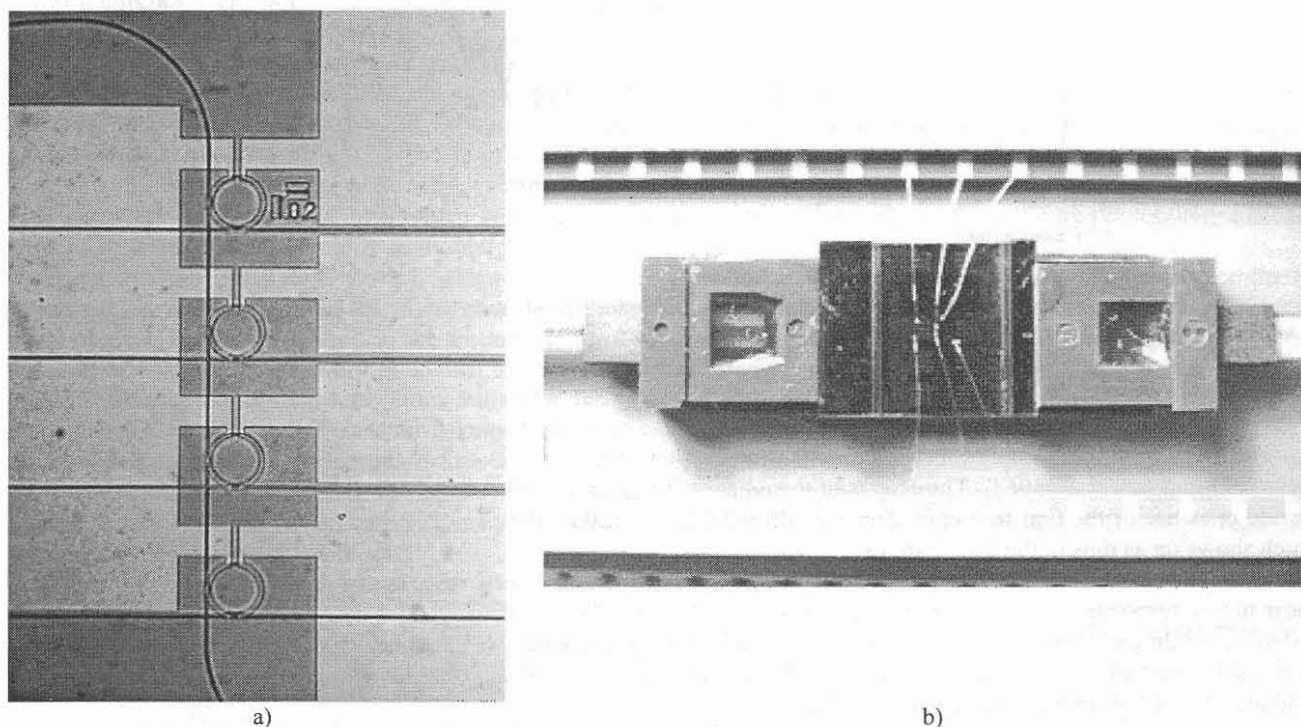


Figure 13: Fabricated ROADMs, a) top view (field of view $1.3 \times 0.5 \text{ mm}^2$), b) fiber pigtailed device

The ROADMs was fabricated by depositing 140 nm LPCVD Si_3N_4 on top of $8 \mu\text{m}$ thermally grown SiO_2 . The Si_3N_4 waveguides were then etched using reactive ion etching (RIE). A $1 \mu\text{m}$ TEOS separation layer was applied next. The ring resonators were then defined by depositing 190 nm Si_3N_4 and RIE. A $4 \mu\text{m}$ thick layer of PECVD SiO_2 was deposited next. The device was then annealed at 1150°C . Subsequently the 200 nm thick Chromium heaters were defined using lift-off. Figure 13 a) shows a close up of a fabricated ROADMs. The central and add/drop waveguides are clearly discernable as well as the omega shaped heater elements on top of the four micro-ring resonators. Figure 13 b) shows a pigtailed and packaged ROADMs chip. The ROADMs chip itself measures $10 \times 9 \text{ mm}$ and contains a total of four ROADMs of which only the center ROADMs is connected.

The pigtailed OADM was measured using a broadband source and an optical spectrum analyzer with a resolution of 0.05 nm . Figure 14.a) shows the normalized responses measured at I_{out} when the broadband source was connected to I_{in} for two distinct configurations which were set by thermally tuning the MRs. In this setup the OADM now drops the channels present on I_{in} to the desired drop ports $I_{\text{Drop}1}$ - $I_{\text{Drop}4}$. These dropped channels are visible as dips in the MR through responses in I_{out} . In the “4-channel configuration” a total heater power of 446 mW was applied to set the MR resonance frequencies on a 100 GHz ITU Grid (spaced at 0.8 nm). The minima of the individual MR through responses are $\approx 12 \text{ dB}$ below the normalized input power level. Thus $\approx 94 \%$ of the input power is extracted. A fit of the individual MR responses to a theoretical MR model showed amplitude coupling constants κ_1 and κ_2 of 0.56 ± 0.04 and 0.44 ± 0.04 respectively at ring losses of $1.5 \pm 0.5 \text{ dB/cm}$. The measured FSR and Finesse were 4.18 nm and 10.3 respectively, giving a FWHM of 0.41 nm ($=51 \text{ GHz}$). The single channel configuration in Fig. 14.a) shows how the responses of the

individual MRs could also be shifted to overlap each other. This configuration could be set while dissipating only 20 mW due to the fact that the untuned MRs already had nearly overlapping resonance frequencies, showing good fabrication reproducibility. The minimum of the combined through response is 30 dB (>99 % extracted).

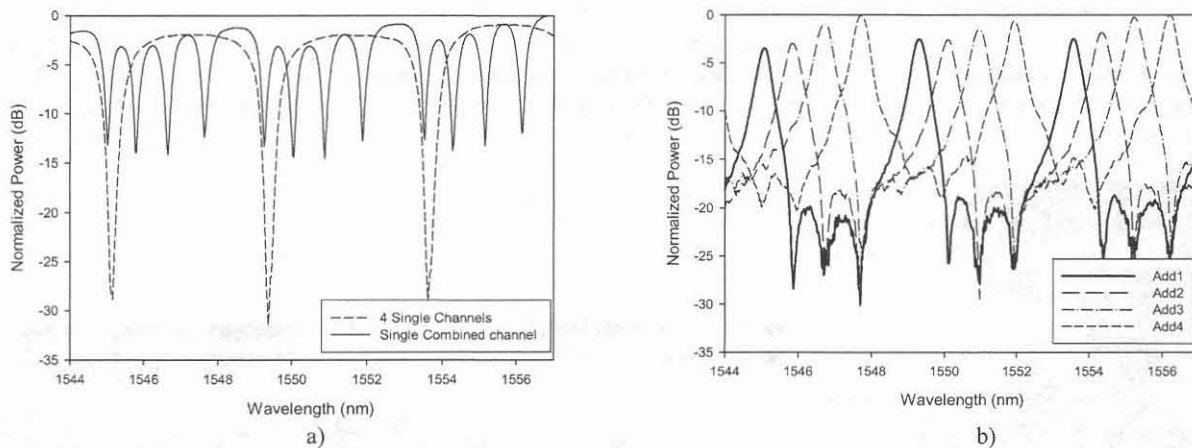


Figure 14: Spectral response of a MR-based ROADM: a) Iout response for a combined-channel and 4-channel OADM configuration; b) Add response for I_{Add1} to I_{Add4} measured at Iout.

Figure 14 b) shows the normalized responses measured at Iout when the broadband source is connected to the different add-ports (I_{Add1} - I_{Add4}). In this configuration the MRs select a channel from these ports and add it to I_{in} . The figure shows that minima of the individual MR drop responses are ≈ 17 dB below the normalized output power level ($\approx 89\%$ of input power dropped). The effects of the adjacent MRs on an add channel can also be observed, for instance in the add response of the first resonator. Here the three MRs that follow the first MR drop power from the main channel which shows up as dips in the Iout response.

The OADM could be reconfigured in < 1 ms due to the fast thermal tuning response of the MRs. A single MR has a linear tuning response and has a maximum tuning range (without heater damage) of ≈ 4.3 nm at a power dissipation of 380 mW, yielding a thermally induced wavelength shift of 11 pm/mW of dissipated heater power. The device shows no measurable thermal crosstalk due to the small heater area, wide (≈ 150 μ m) heater separation and the high thermal conductivity (161 W/m/K) of the silicon substrate.

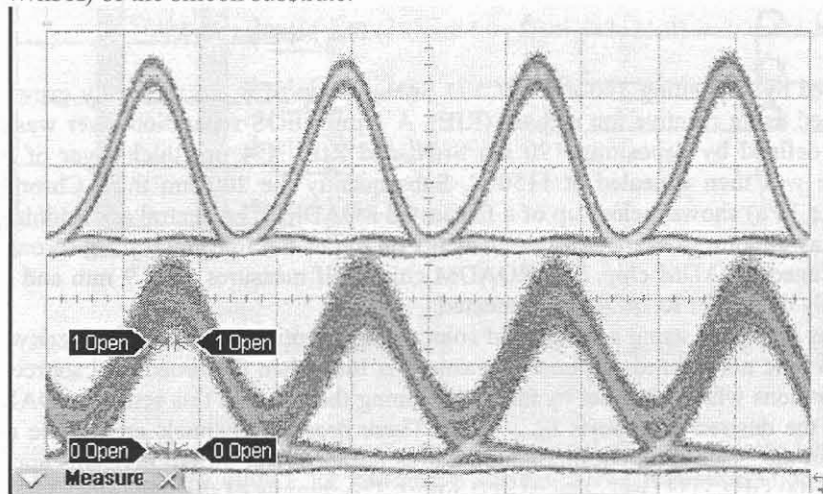


Fig. 15: Eye pattern at 40 Gbit/s obtained at the drop port of the ROADM depicted in Figures 13 and 14

Recently high speed measurements on the OADM have been performed in cooperation with the HHI in Berlin²². Figure 15 shows the measured EYE patterns of 40 Gbit/s incoming signal (top) and at the Drop1 port (bottom) while the

MR was tuned to the wavelength of the tunable laser. Clean EYE openings can be seen allowing error free detection with a slight power penalty of 1 dB. The Drop1 response shows an increase in noise caused by the EDFAs needed to overcome the relative high insertion loss. Furthermore at the crossings some inter-symbol-interference can be seen, but the EYE stays open enough for detection. All other ports, both drop and add showed similar responses.

4. OTHER FUNCTIONS IMPLEMENTED IN OPTICAL MICRORESONATORS

In the foregoing section MRs were applied as optical filters, modulators and ROADM. In the following two other applications, light generation and optical sensing, will be addressed to demonstrate their potential as building blocks for VLSI photonics.

4.1 Lightsources based on microresonators

With the availability of convenient optical active materials it is straightforward to apply microring resonators as ultra-compact ring lasers. The groups of Vahala and Polman demonstrated Er-doped silica laser with ultralow threshold pump power below $10 \mu\text{W}$ ²³. The laser consists of a microtoroid resonator with a diameter of $40 \mu\text{m}$ with ultra-smooth sidewalls. These were obtained by surface tension induced smoothing of a silica disk irradiated by an intense CO_2 laser. For applications as lightsource in VLSI photonics a more controlled process including photolithographically defined port waveguides is highly desirable.

In our group Dekker et al.²⁴ work with rare earth-doped nanoparticles dispersed in polymers with very promising properties for amplification in active integrated optical devices. Especially the rare earths neodymium and erbium are of great interest, because they emit in the second and third window of optical communication systems, respectively. It has been reported that LaF_3 is a very good host for rare earth incorporation and because of its low phonon energy it exhibits a wide transparency band from 0.2 to $11 \mu\text{m}$. Polymer waveguide materials have the advantage of being low-cost and tunable in many ways with respect to their properties and ways of processing. To overcome the insolubility problem of inorganic rare earth salts in polymers, Stouwdam et al.²⁵ developed neodymium doped LaF_3 nanoparticles with organic ligands that do dissolve well in polymers. By combining the broad range of attractive polymer properties and the relatively long lifetime of rare earth dopants in inorganic nanoparticles, a considerable amount of flexibility regarding materials properties can be achieved.

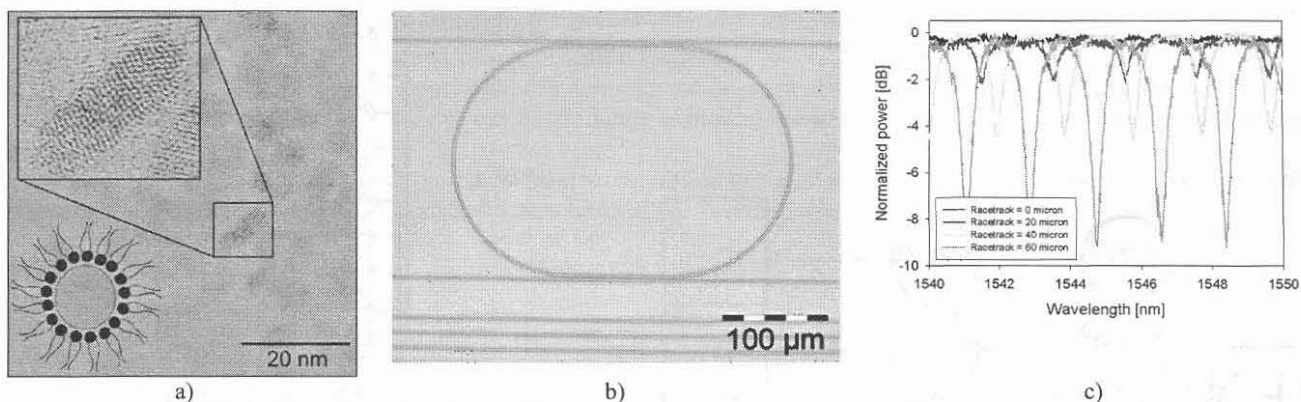


Figure 15: Results of $\text{LaF}_3:\text{Nd}$ nanoparticles dispersed in polymer waveguiding structures: a) TEM picture of the nanoparticles; b) MR realized in photodefinable polymer doped with these nanoparticles; c) spectral response of the through port with increasing length of the racetrack

In order to demonstrate the approach, some first results on MRs are presented. In Figure 15.a) a TEM picture is given showing the $\text{LaF}_3:\text{Nd}$ nanoparticles with a diameter of 5-10 nm. The inset with the higher magnification demonstrates the crystalline character of the nanoparticles. The organic ligands are shown that act as a kind of flexible spacer to avoid clustering and enhance solubility. In Fig. 15.b) a microscope photo is given of a racetrack MR obtained by photodefinable polymer of which the index of refraction was matched to the index of LaF_3 to avoid scattering losses. On the same mask devices with different racetrack length were positioned in order to vary the coupler length and consequently the effective coupling strength. The spectra obtained of a set of MRs are given in Figure 15.c) showing decreasing dips for increasing coupling constant. Experiments are in progress to show decreased losses by optical pumping and eventually lasing.

4.2 The microresonator as optical sensor

Optical sensing in general is based on changes on the optical properties of materials within the optical circuitry due to changes in the environment. Excluding sensors that in the sensing process generate light, one mostly tries to detect changes in the refractive index or the absorption at a certain wavelength. Using interferometric sensors, changes as low as 10^{-9} in the index of refraction can be measured²⁶. Microresonators offer some unique properties for optical sensing as they are very sensitive to small changes in the refractive index. They are very small and the measuring volume can be below 1 pL (10^{-12} L) making them ideal for Lab-on-a-chip applications.

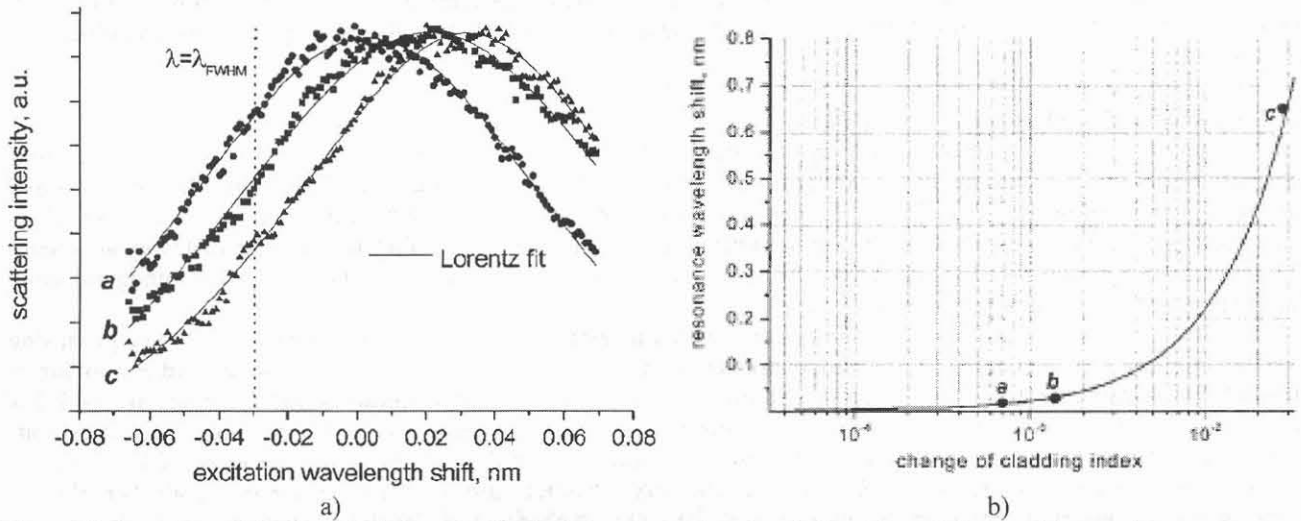


Figure 16: Experimental results of Krioukov et al.⁹ of microresonator based optical sensing of glucose; (a) scattering spectra near a resonance recorded by fine laser tuning for "a" water, "b" 0.5% glucose and "c" 1% glucose in the cladding; (b) measured shifts in resonance wavelength for three claddings for "a" 0.5% glucose, "b" 1% glucose and "c" EtOH ($n = 1.36$)

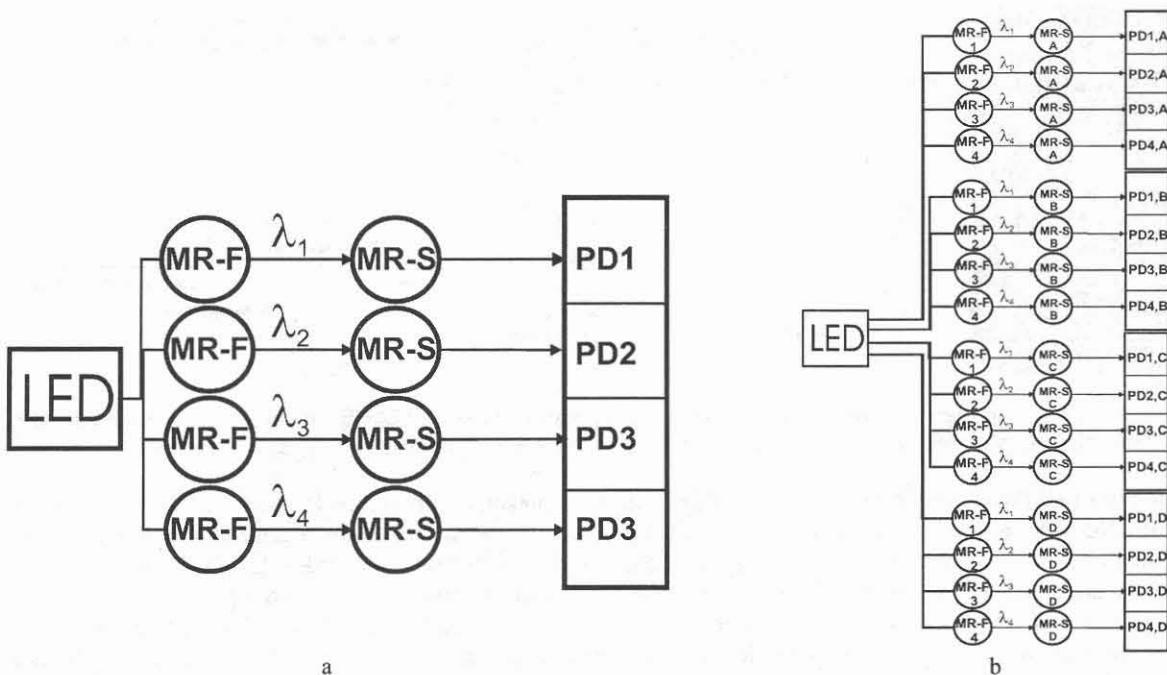


Figure 17: Schematic lay-out of compact optical sensor chip without need of external optical apparatus; LED: broad band source, for example Light Emitting Diode, MR-F: microresonator used as optical filter, MR-S: microresonator used as optical sensor, PD: Photo Diode. (a) version with identical microresonators as sensors; (b) multi-sensor chip with 4 different sets of sensing arrays.

Krioukov et al.⁹ demonstrated the feasibility of optical sensing by measuring the wavelength dependence of the scattered light of a microresonator that - for a small wavelength range - is proportional to the light power inside the resonator. In a practical design that power could be much easier be determined by measuring the intensity at the drop port. For the proof of principle they immersed the microresonator in glucose solution of various concentrations. Fig. 16 gives the result for pure water and a 0.5 and 1% glucose solution. In their not yet optimized set-up refractive index changes well below 10^{-4} could be detected. Working with high finesse resonators and advanced curve fitting, detection of changes as low as 10^{-9} becomes feasible. With further reduction of the resonator diameter the measuring volume could be even larger reduced so that single or at least few molecule detection would be possible. In a second paper Krioukov et al.²⁷ demonstrated the use of optical microresonators for enhanced optical spectroscopy and sensing. Also here the small sensing volume make this kind of sensors attractive devices for high-sensitivity sensing and detection down to the single molecule level.

Due to the small area needed for a MR advanced sensor arrays become feasible that in addition perform optical data processing. Consider, for example, a sensor chip where microresonators with the typical wavelength response as depicted in Fig. 2 are employed as wavelength filter together with a set of microresonators as sensors, see Fig. 17.a). In this case, a cheap broadband light source like a LED could be used together with silicon photodiodes fabricated in CMOS technology. An additional advantage is the inherent possibility for temperature compensation, as only one of the microresonators for each wavelength is exposed to the measurand. Complexity increases if one starts incorporating multisensor functions, Fig. 17.b). In this way an optical nose or optical tongue with only a modest power supply and without optical peripheral equipment would become feasible.

5. CONCLUSIONS

With the foregoing the basic principles and the potential of optical microresonators for a number of applications have been shown. It is, of course, still too early to speak about VLSI photonics, but microresonators can be considered as promising candidates for the basic building blocks needed in optical circuitry. Much work has still to be done in a number of fields:

- (i) new or improved materials that allow active optical functions,
- (ii) better design tools for single devices as well systems,
- (iii) better and more reliable technology
- (iv) improved measurement and characterization methods
- (v) system studies to allow applications in communication, optical sensing and other upcoming fields.

In this way the potential of nanophotonics can be gradually exploited resulting in complex, mass-produced and low-cost optical circuits

The examples presented have mostly be taken from work carried out at the IOMS group of the MESA⁺ institute of the University of Twente, often in collaboration with other MESA⁺ groups.

ACKNOWLEDGMENTS

The authors would like to thank Anton J.F. Hollink, Henry Kelderman, Paul V. Lambeck, Gabriel Sengo, Henk van Wolferen and Kerstin Wörhoff for their contribution in the research described in this paper.

Financial support is acknowledged of the Dutch Science Foundations FOM, STW and BSIK Freeband and the EC project NAIS.

REFERENCES

¹ S. Téral, *Fibre System Europe*, June 2005, p 8.

² see, for example, D.J.W. Klunder, E. Krioukov, F.S. Tan, T. van der Veen, H.F. Bulthuis, G. Sengo, C. Otto, H.J.W.M. Hoekstra and A. Driessen, "Vertically and laterally waveguide-coupled cylindrical microresonators in Si₃N₄ on SiO₂ technology", *Appl. Phys. B*, **73**, 603-608 (2001).

³ B.E. Little, H.A. Haus, J.S. Foresi, L.C. Kimerling, E.P. Ippen and D.J. Ripin, "Wavelength switching and routing using absorption and resonance", *IEEE Phot. Techn. Letters*, **10**, 816-818 (1998).

- ⁴ For an overview, see F. Michelotti, A. Driessen and M. Bertolotti (eds.) *Microresonators as building blocks for VLSI photonics*, AIP Conf. Proc. Vol. 709, 451 p. (2004).
- ⁵ see for more details, D.J.W. Klunder, *Photon Physics in Integrated Optics Microresonators*, Pd.D. thesis, University of Twente, 135 p (2002).
- ⁶ Y. Shi, C. Zhang, H. Zhang, J.H. Bechtel, L.R. Dalton, B.H. Robinson and W.H. Steier, "Low (sub-1-volt) halfwave voltage polymeric electro-optic modulators achieved by controlling chromophore shape", *Science* **288**, 119-122 (2000).
- ⁷ F.C. Blom, D.R. van Dijk, H.J.W.M. Hoekstra, A. Driessen and Th.J.A. Popma, "Experimental study of integrated-optics microcavity resonators: Toward an all-optical switching device", *Appl. Phys. Letters* **71**, 747-749 (1997).
- ⁸ G.N. Nielson, D. Seneviratne, F. Lopez-Royo, P.T. Rakich, Y. Avrahami, M.R. Watts, H.A. Haus, H.L. Tuller, and G. Barbastathis, "Integrated Wavelength-Selective Optical MEMS Switching Using Ring Resonator Filters" *IEEE Phot. Techn. Letters* **17**, 1190-1192 (2005).
- ⁹ E. Krioukov, D.J.W. Klunder, A. Driessen, J. Greve, C. Otto, "Sensor based on an integrated optical microcavity", *Optics Letters* **27**, 512-514, (2002).
- ¹⁰ EC project IST-2002-28018, <http://www.mesaplus.utwente.nl/nais/>
- ¹¹ D. Geuzebroek, E.J. Klein, H. Kelderman, N. Baker and A. Driessen, "Compact wavelength-selective switch for Gigabit filtering in access networks", *IEEE Phot. Techn. Letters*, **17**, 336-338 (2005).
- ¹² R. Meijerink, D.H. Geuzebroek, E.J. Klein, H. Kelderman, R. Dekker, M.B.J. Diemer and A. Driessen, "Optimization of driving signal for thermal modulation of a microring resonator," in *Proc. Symp. LEOS Benelux Chapter.*, 85-88 (2003).
- ¹³ D.H. Geuzebroek, E.J. Klein, H. Kelderman, F.S. Tan, D.J.W. Klunder and A. Driessen., "Thermally tuneable, wide FSR switch based on micro-ring resonators," in *Proc. Symp. IEEE/LEOS Benelux, Chapter*, 155-158 (2002).
- ¹⁴ K. Worhoff, L.T.H. Hilderink, A. Driessen and P.V. Lambeck, "Silicon oxynitride—A versatile material for integrated optics applications," *J. Electrochem. Soc.*, vol. 149, no. 8, F85-F91 (2002).
- ¹⁵ D. Marcuse, *Principles of Optical Fiber Measurements*, New York, Academic Press, (1981).
- ¹⁶ A. Leinse, M.B.J. Diemeer, A. Rousseau and A. Driessen, "A novel high speed polymeric eo modulator based on a combination of a micro-ring resonator and an MZI", *IEEE Photon. Technol. Lett.*, to be published, Oct. (2005).
- ¹⁷ Rabiei P, Steier WH, Cheng Zhang, Dalton LR. "Polymer Micro-Ring filters and modulators", *J. of Lightw. Techn.*, **20**, 1968-1975, (2002).
- ¹⁸ Nagtegaele P, Brasselet E, Zyss J, "Anisotropy and dispersion of a Pockels tensor: a benchmark for electro-optic organic thin-film assessment", *Journal of the Optical Society of America B*, vol **20**, 1932-1936 (2003).
- ¹⁹ E. Klein, D.H. Geuzebroek, H. Kelderman, G. Sengo, N. Baker and A. Driessen, "Reconfigurable optical add-drop multiplexer using microring resonators", *Proc. ECIO '05*, Grenoble 2005.
- ²⁰ B.E. Little, S.T. Chu, W. Pan and Y. Kokubun, "Microring resonator arrays for VLSI photonics", *IEEE Phot. Techn. Letters*, **12** 323-325 (2000).
- ²¹ S.T.Chu, B.E. Little, W.G. Pan, T. Kaneko, S. Sato and Y. Kokubun, "An Eight Channel Add-Drop Filter Using Vertically Coupled Microring Resonators over a Cross Grid", *IEEE Phot. Techn. Letters*, **11**, 691-693 (1999).
- ²² D.H. Geuzebroek, E.J. Klein, H. Kelderman, C. Bornholdt and A. Driessen, "40 Gbit/s reconfigurable optical add-drop multiplexer base don microring resonators", *Proc. ECOC 05*, to be published (2005).
- ²³ A. Polman, B. Min, J. Kalkman, T.J. Kippenberg and KJ Vahala, "Ultra low-threshold erbium-implanted toroidal microlaser on silicon", *Appl. Phys. Letters* **84**, 1037-1039 (2004).
- ²⁴ R. Dekker, D.J.W. Klunder, A. Borreman, M.B.J. Diemeer, K. Wörhoff, and A. Driessen, J.W. Stouwdam and F.C.J.M. van Veggel "Stimulated emission and optical gain in LaF₃:Nd nanoparticle-doped polymer-based waveguides", *Appl. Phys. Letters*, **85**, 6104-6106 (2004).
- ²⁵ J.W. Stouwdam, G.A. Hebbink, J. Huskens, and F.C.J.M. van Veggel, "Lanthanide-doped nanoparticles with excellent luminescent properties in organic media", *Chem. Mater.* **15**, 4604-4616 (2003).
- ²⁶ R.G. Heideman and P.V. Lambeck, "Remote opto-chemical sensing with extreme sensitivity: design, fabrication and performance of a pigtailed integrated optical phase-modulated Mach-Zehnder interferometer system", *Sensors & Actuators B* **61**, 100-127 (1999).
- ²⁷ E. Krioukov E., D.J.W. Klunder, A. Driessen, J. Greve, C. Otto, "Integrated optical microcavities for enhanced evanescent-wave spectroscopy", *Optics Letters*, **27**, 1504-1506 (2002).

Integrated Optics: Theory and Applications


Tadeusz Pustelny
Paul V. Lambeck
Christophe Gorecki
Chairs/Editors

31 August–2 September 2005
Warsaw, Poland

Organized by
SPIE Poland Chapter
SPIE Europe
Warsaw University of Technology (Poland)

Sponsored by
NEMO—Network of Excellence on Micro-Optics
European Office of Aerospace Research and Development



Volume 5956
 **The International Society
for Optical Engineering**

ISSN 0277-786X
ISBN 0-8194-5963-1